

plastid genome: the lack of RNA editing leads to a mutant phenotype. *EMBO J.* **13**, 4623–4628 (1994).

3. Sasaki, Y., Kozaki, A., Ohmori, A., Iguchi, H. & Nagano, Y. Chloroplast RNA editing required for functional acetyl-CoA carboxylase in plants. *J. Biol. Chem.* **276**, 3937–3940 (2000).
4. Chaudhuri, S., Carrer, H. & Maliga, P. Site-specific factor involved in the editing of the *psbL* mRNA in tobacco plastids. *EMBO J.* **14**, 2951–2957 (1995).
5. Hirose, T. & Sugiura, M. Involvement of a site-specific trans-acting factor and a common RNA-binding protein in the editing of chloroplast mRNAs: development of a chloroplast *in vitro* RNA editing system. *EMBO J.* **20**, 1144–1152 (2001).
6. Shikanai, T. *et al.* Directed disruption of the tobacco *ndhB* gene impairs cyclic electron flow around photosystem I. *Proc. Natl Acad. Sci. USA* **95**, 9705–9709 (1998).
7. Munekage, Y. *et al.* Cyclic electron flow around photosystem I is essential for photosynthesis. *Nature* **429**, 579–582 (2004).
8. Hashimoto, M., Endo, T., Peltier, G., Tasaka, M. & Shikanai, T. A nucleus-encoded factor, CRR2, is essential for the expression of chloroplast *ndhB* in *Arabidopsis*. *Plant J.* **36**, 541–549 (2003).
9. Shikanai, T., Munekage, Y., Shimizu, K., Endo, T. & Hashimoto, T. Identification and characterization of *Arabidopsis* mutants with reduced quenching of chlorophyll fluorescence. *Plant Cell Physiol.* **40**, 1134–1142 (1999).
10. Aubourg, S., Boudet, N., Kreis, M. & Lechary, A. In *Arabidopsis thaliana*, 1% of the genome codes for a novel protein family unique to plants. *Plant Mol. Biol.* **42**, 603–613 (2000).
11. Small, I. D. & Peeters, N. The PPR motif—a TPR-related motif prevalent in plant organellar proteins. *Trends Biochem. Sci.* **25**, 46–47 (2000).
12. Lurin, C. *et al.* Genome-wide analysis of *Arabidopsis* pentatricopeptide repeat proteins reveals their essential role in organelle biogenesis. *Plant Cell* **16**, 2089–2103.
13. Fisk, D. G., Walker, M. B. & Barkan, A. Molecular cloning of the maize gene *crp1* reveals similarity between regulators of mitochondrial and chloroplast gene expression. *EMBO J.* **18**, 2621–2630 (1999).
14. Meierhoff, K., Felder, S., Nakamura, T., Bechtold, N. & Schuster, G. HCF152, an *Arabidopsis* RNA binding pentatricopeptide repeat protein involved in the processing of chloroplast *psbB-psbT-psbH-petB-petD* RNAs. *Plant Cell* **15**, 1480–1495 (2003).
15. Yamazaki, H., Tasaka, M. & Shikanai, T. PPR motifs of the nucleus-encoded factor, PGR3, function in the selective and distinct steps of chloroplast gene expression in *Arabidopsis*. *Plant J.* **38**, 152–163 (2004).
16. Williams, P. M. & Barkan, A. A chloroplast-localized PPR protein required for plastid ribosome accumulation. *Plant J.* **36**, 675–686 (2003).
17. Manthey, M. G. & McEwen, J. E. The product of the nuclear gene *PET309* is required for translation of mature mRNA and stability or production of intron-containing RNAs derived from the mitochondrial *COX1* locus of *Saccharomyces cerevisiae*. *EMBO J.* **14**, 4031–4043 (1995).
18. Coffin, J. W., Dhillon, R., Ritzel, R. G. & Nargang, F. E. The *Neurospora crassa cya-5* nuclear gene encodes a protein with a region of homology to the *Saccharomyces cerevisiae* PET309 protein and is required in a post-transcriptional step for the expression of the mitochondrially encoded COXI protein. *Curr. Genet.* **32**, 273–280 (1997).
19. Bentolila, S., Alfonso, A. A. & Hanson, M. R. A pentatricopeptide repeat-containing gene restores fertility to cytoplasmic male-sterile plants. *Proc. Natl Acad. Sci. USA* **99**, 10887–10892 (2002).
20. Kazama, T. & Toriyama, K. A pentatricopeptide repeat-containing gene that promotes the processing of aberrant *atp6* RNA of cytoplasmic male-sterile rice. *FEBS Lett.* **544**, 99–102 (2003).
21. Koizuka, N. *et al.* Genetic characterization of a pentatricopeptide repeat protein gene, *orf687*, that restores fertility in the cytoplasmic male-sterile Kosena radish. *Plant J.* **34**, 407–415 (2003).
22. Lutz, K. A. & Maliga, P. Lack of conservation of editing sites in mRNAs that encode subunits of the NAD(P)H dehydrogenase complex in plastids and mitochondria of *Arabidopsis thaliana*. *Curr. Genet.* **40**, 214–219 (2001).
23. Neckermann, K., Zeltz, P., Igloi, G. L., Kössel, H. & Maier, R. M. The role of RNA editing in conservation of start codons in chloroplast genomes. *Gene* **146**, 177–182 (1994).
24. Hirose, T. & Sugiura, M. Both RNA editing and RNA cleavage are required for translation of tobacco chloroplast *ndhD* mRNA: a possible regulatory mechanism for the expression of a chloroplast operon consisting of functionally unrelated genes. *EMBO J.* **16**, 6804–6811 (1997).
25. del Campo, E. M., Sabater, B. & Martin, M. Post-transcriptional control of chloroplast gene expression. Accumulation of stable *psaC* mRNA is due to downstream RNA cleavages in the *ndhD* gene. *J. Biol. Chem.* **277**, 36457–36464 (2002).
26. Chateigner-Boutin, A.-L. & Hanson, M. R. Developmental co-variation of RNA editing extent of plastid editing sites exhibiting similar *cis*-elements. *Nucleic Acids Res.* **31**, 2586–2594 (2003).
27. Guera, A., Nova, P. G. & Sabater, B. Identification of the Ndh (NAD(P)H-plastoquinone-oxidoreductase) complex in etioplast membranes of barley: changes during photomorphogenesis of chloroplasts. *Plant Cell Physiol.* **41**, 49–59 (2000).
28. Keegan, L. P., Gallo, A. & O’Connell, M. A. The many roles of an RNA editor. *Nature Rev. Genet.* **2**, 869–878 (2001).
29. Miyamoto, T., Obokata, J. & Sugiura, M. A site-specific factor interacts directly with its cognate RNA editing site in chloroplast transcripts. *Proc. Natl Acad. Sci. USA* **101**, 48–52 (2004).
30. Glegé, P. & Brennicke, A. RNA editing in *Arabidopsis* mitochondria effects 441 C to U changes in ORFs. *Proc. Natl Acad. Sci. USA* **96**, 15324–15329 (1999).

Supplementary Information accompanies the paper on www.nature.com/nature.

Acknowledgements We thank M. Miyata and E. Habe for their technical assistance; T. Endo, G. Peltier and the late A. Watanabe for antibodies; and J. Obokata for suggestions. T. Shikanai was supported by grants from JSPS and Ministry of Education, Sports, Culture, Science and Technology, Japan.

Competing interests statement The authors declare that they have no competing financial interests.

Correspondence and requests for materials should be addressed to T.S. (shikanai@agr.kyushu-u.ac.jp).

Molecular dynamics of cyclically contracting insect flight muscle *in vivo*

Michael Dickinson¹, Gerrie Farman^{2*}, Mark Frye^{1*}, Tanya Bekyarova², David Gore², David Maughan³ & Thomas Irving²

¹Department of Bioengineering, California Institute of Technology, Pasadena, California 91125, USA

²BioCAT and CSRR, Department BCPS, Illinois Institute of Technology, Chicago, Illinois 60616, USA

³Department of Molecular Physiology and Biophysics, University of Vermont, Burlington, Vermont 05405, USA

* Present addresses: Department of Physiology and Biophysics, University of Illinois at Chicago, Chicago, Illinois 60612, USA (G.F.); Department of Physiological Science, University of California, Los Angeles, Los Angeles, California 90095, USA (M.F.).

Flight in insects—which constitute the largest group of species in the animal kingdom—is powered by specialized muscles located within the thorax. In most insects each contraction is triggered not by a motor neuron spike but by mechanical stretch imposed by antagonistic muscles¹. Whereas ‘stretch activation’ and its reciprocal phenomenon ‘shortening deactivation’ are observed to varying extents in all striated muscles, both are particularly prominent in the indirect flight muscles of insects¹. Here we show changes in thick-filament structure and actin–myosin interactions in living, flying *Drosophila* with the use of synchrotron small-angle X-ray diffraction. To elicit stable flight behaviour and permit the capture of images at specific phases within the 5-ms wingbeat cycle, we tethered flies within a visual flight simulator². We recorded images of 340 μs duration every 625 μs to create an eight-frame diffraction movie, with each frame reflecting the instantaneous structure of the contractile apparatus. These time-resolved measurements of molecular-level structure provide new insight into the unique ability of insect flight muscle to generate elevated power at high frequency.

The asynchronous indirect flight muscles (IFMs) of insects have served as a valuable model system for general structural studies of muscle because of the well-ordered arrangement of the contractile lattice. X-ray diffraction studies (for example refs 3–6) and electron microscopy studies (for example refs 3, 5, 7, 8) of glycerol-extracted fibres from the giant waterbug, *Lethocerus* sp., in combination with crystallographic information, have produced a high-resolution view of actin–myosin interactions^{6,8,9}. Previous synchrotron X-ray diffraction studies of *Drosophila*¹⁰ demonstrated the feasibility of obtaining patterns from intact IFMs in live flies. Because of the similarity of the IFM structures, the extensive literature from preparations of *Lethocerus* IFM *in vitro* can be used as a framework for interpreting changes in X-ray diffraction patterns obtained from living, flying *Drosophila*. Here we optically tracked the motion of the beating wings in real time and triggered the X-ray exposure at specific phases of the wingbeat cycle (Fig. 1). The beam was focused on the dorsal longitudinal muscles (DLMs), the IFMs that contract during the downstroke. The tethered animal was surrounded by an electronic display of vertical stripes, the motion of which was controlled by the insect’s own wing motion under closed-loop conditions². This arrangement maintained a stable wingbeat frequency, permitting accurate shuttering at precise phase points within the contraction cycle. By progressing through the wingbeat, we reconstructed a movie of X-ray diffraction images from the DLMs. Figure 2 shows examples of such images obtained from a single *Drosophila metleri* (the full sequence is shown as an animation in Supplementary Video 1). The cyclical changes in the intensities and positions of the major reflections reflect the cyclical binding,

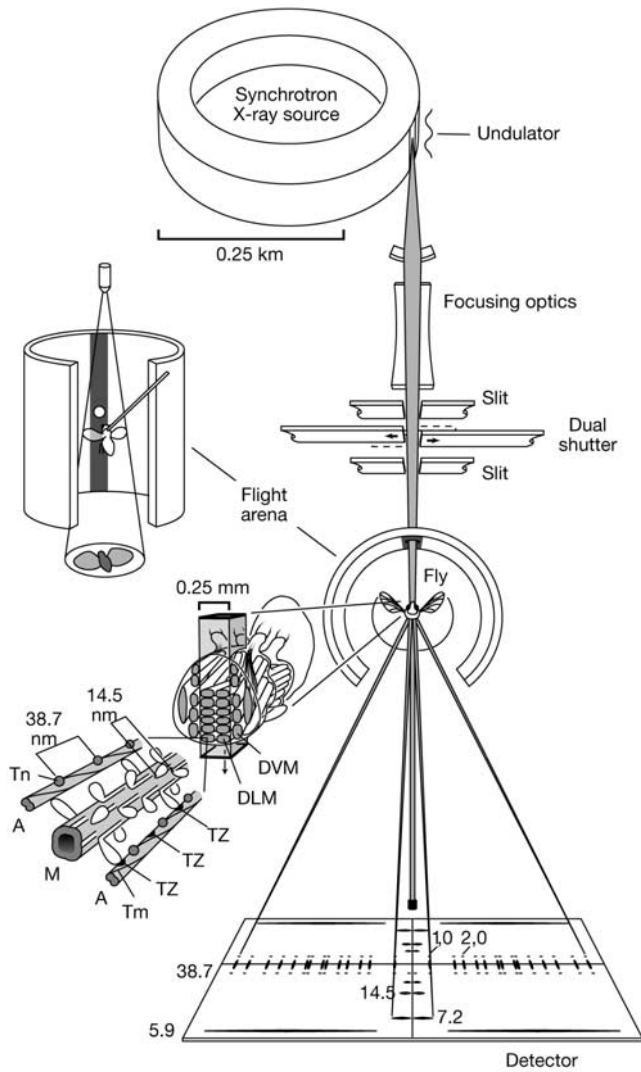


Figure 1 Experimental arrangement. The position of the fly is shown relative to the flight arena and the X-ray optical path. The locations of the DLMs and DVMs with respect to the incident X-ray beam are indicated in the expanded view. Periodic structures of the filament lattice that give rise to the features seen in diffraction patterns are also indicated (Tn, troponin complex; Tm, tropomyosin). Note the axial rise at 14.5 nm between myosin (M) heads along the thick filaments and the location of target zones (TZ) for the binding of myosin heads to actin (A) halfway between troponins, which are spaced every 38.7 nm along the thin filament.

tilting and release of myosin heads on actin target zones during the wingbeat (Fig. 3).

In vertebrate muscle, the intensity of the 14.5-nm meridional reflection has been shown to arise mainly from the axial projection of the density of myosin heads onto the thick-filament backbone^{11–13}, whereas higher-order reflections, such as that at 7.2 nm, are thought to arise from periodic features within the backbone itself^{14,15}. Therefore, changes in the position of the 7.2-nm reflection provide a measure of thick-filament backbone strain, whereas motion of the 14.5-nm reflection is caused by changes in the position of the centre of mass of the myosin heads in series with the backbone strain. Figure 3a shows the relationship of the spacing of the 7.2-nm and 14.5-nm meridional reflections relative to rest throughout the upstroke–downstroke cycle of the wings. Both spacings are tightly coupled to the lengthening–shortening cycle of the DLMs¹⁶, and both increase as the DLMs are extended and decrease as they shorten. These spacing changes are in phase with each other and with the length cycle of the DLMs, suggesting that strains in the thick filaments are elastically coupled to sarcomere length, which is consistent with previous observations on passively stretched vertebrate muscle¹⁷. The amplitude of these cyclic strains, measured by comparing the 0.3 and 0.93 phase points (as indicated by two dashed lines in Fig. 3a), are different for the two reflections. The 14.5-nm reflection shows a 0.4% change (0.06 nm per repeat), twice the 0.2% change (0.014 nm per repeat) measured for the 7.2-nm reflection ($P < 0.05$). The larger movement of the 14.5-nm reflection suggests that the centres of mass, presumably the catalytic domains of the myosin heads, separate by an additional ~ 0.03 nm from each other as they are pulled towards the Z-disk by the thin filaments. Because the thin filaments are compliant, this shear force should be greatest near the Z-disk and diminish towards the M-line. This gradient would result in an increased separation of attached heads, which might explain the greater spacing change of the 14.5-nm reflection relative to the 7.2-nm reflection. However, this interpretation is complicated by the fact that the number of attached heads increases during extension, as discussed below. Nevertheless, the elastic deformation of the thick filaments during muscle lengthening immediately suggests a mechanism by which appreciable potential energy is stored in the muscle as elastic strain, available for conversion into kinetic energy during the shortening phase. Elastic storage has been proposed as an important feature of the flight motor that minimizes the inertial power costs of accelerating the wings back and forth in each wingbeat^{18–20}. These results would suggest that at least part of this storage takes place within the myofilaments themselves.

Unlike in *Lethocerus*, the 14.5-nm meridional reflection in *Drosophila* is weak in resting intact muscle, which is consistent with its relatively disordered appearance in electron micrographs²¹.

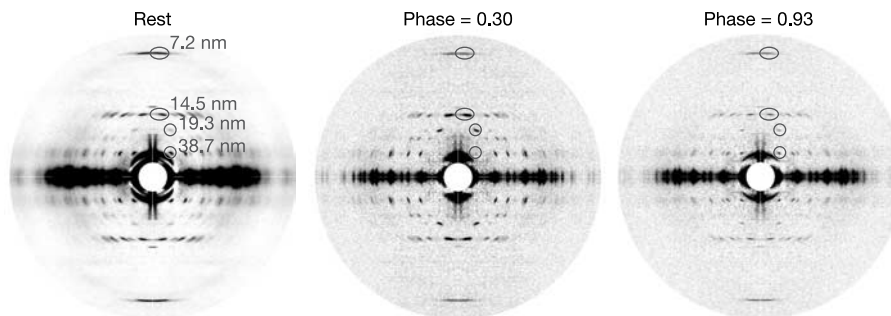


Figure 2 X-ray patterns from live flies. Shown are background-subtracted X-ray diffraction patterns from live *Drosophila metleri* at rest, near the end of lengthening (0.3 phase) and near the end of shortening (0.93 phase). Note the evident increase in overall ordering of the 0.3 phase with respect to the 0.93 phase (vertical dotted lines). The

positions of the 7.2-nm and 14.5-nm near-meridional reflections and the 38.7-nm and 19.3-nm reflections on the first row line are indicated. The 14.5-nm and 7.2-nm reflections in *Drosophila* sp. appear split because of axial stagger of thick filaments¹⁰. The resting pattern had a tenfold greater exposure.

Throughout the wingbeat cycle, the intensity of the 14.5-nm reflection varies by 400%, in phase with thick-filament strain (Fig. 3b). In contrast, the intensity of the 7.2-nm reflection undergoes only a 40% increase in intensity over the same period, indicating that the large change in the 14.5-nm reflection is not an artefact of the general ordering or alignment of the tissue. The intensity of the 14.5-nm reflection may be attributed to changes in the angle between the crossbridges and the long axes of the thick filaments, as well as to changes in the angular dispersion of the crossbridges with respect to that axis^{11,13,22}. The fourfold rise in the intensity of the 14.5-nm reflection can therefore be explained by the crossbridges becoming progressively more ordered and more

perpendicular to the thick-filament backbone during muscle lengthening. The corresponding decrease in intensity at 14.5 nm during shortening is consistent with the expected lever-arm tilting during crossbridge powerstrokes.

Figure 3c shows the variation in intensity of the 38.7-nm and 19.3-nm reflections on the first row line. The 38.7-nm reflection is thought to be due to the troponin complexes located every 38.7 nm along the thin filament with contributions from actin–myosin interactions in active muscle. In contrast, the 19.3-nm reflection is interpreted specifically as a marker for the interaction of myosin heads with the actin helix at sterically optimal target zones located midway between troponin repeats⁵. For stretch-activated *Lethocerus* IFM *in vitro*, it has been shown⁵ that myosin labelling at target zones increases the 19.3-nm reflection and diminishes the 38.7-nm reflection through destructive interference. Consistent with this is the observation that the 19.3-nm reflection in intact flies rises during stretching of the DLMs and declines during shortening, whereas the 38.7-nm reflection shows the opposite behaviour (Fig. 3c). The increase in intensity of the 19.3-nm reflection during lengthening provides direct evidence that a substantial fraction of the total number of cycling crossbridges form attachments at actin target zones as the DLMs are being stretched by the antagonistic dorsal-ventral muscles (DVMs). The importance of cycling crossbridges during lengthening in the underlying mechanics of stretch activation was first suggested by Squire²³ and accords with recent work²⁴ showing that some Ca²⁺ activated bridges must be attached to the thin filament before stretch activation can occur.

In both *Lethocerus* and *Drosophila* IFM, two isoforms of troponin C exist, one regulated by stretch (F1), the other by Ca²⁺ (F2)²⁵. Both are assumed to relieve the inhibitory effect of troponin I on crossbridge formation by altering the position of tropomyosin to uncover actin-binding sites. The myosin heads that attach to actin during lengthening will be pulled towards the Z-disk, opposite to their direction of motion during powerstrokes. These strained crossbridges are therefore likely candidates for the 'sensors' that activate the stretch-dependent F1 isoform of troponin C, leading to the rapid binding of myosin heads at target zones as indicated by the observed changes in the 19.3-nm reflection intensity²⁴. Future time-resolved experiments that record the second actin layer line, a marker for tropomyosin movement during thin-filament activation, could serve to confirm this hypothesis.

During the transition from lengthening to shortening, muscle contraction must transiently approach isometric conditions (Fig. 3a). At this point, the 19.3-nm and 14.5-nm reflection intensities are maximal, indicating that a large proportion of heads are attached, well ordered and nearly perpendicular to the long axis of the thick filaments, an arrangement similar to isometrically contracting *Lethocerus* IFM *in vitro*²⁶ and to isolated frog muscle^{13,27}. The rapid decline in intensity at 14.5 nm at the onset of shortening suggests that the first crossbridge powerstrokes are roughly synchronous. In five of six preparations we detected a rapid decrease in the intensity of the 19.3-nm immediately after the onset of shortening, followed by a transient recovery (Fig. 3c). An interpretation of the initial decrease is that the first set of synchronously acting crossbridges detaches at the end of their powerstroke, followed by the attachment of another population, which immediately undergo powerstrokes that continue to shorten the muscle. Multiple powerstrokes are required during the shortening phase of the wingbeat because the relative axial displacement of the thick and thin filaments during shortening, about 3.5% or about 58 nm (ref. 16), is much longer than any single crossbridge step displacement (about 7 nm)²⁸. During shortening, the occupancy of target zones by bound crossbridges, as indicated by the intensity of the 19.3-nm reflection, remains high until roughly halfway through the downstroke, whereupon it decreases rapidly, concurrent with both the observed decrease in thick-filament strain (Fig. 3a) and the postulated decrease in strain of actin-bound crossbridges

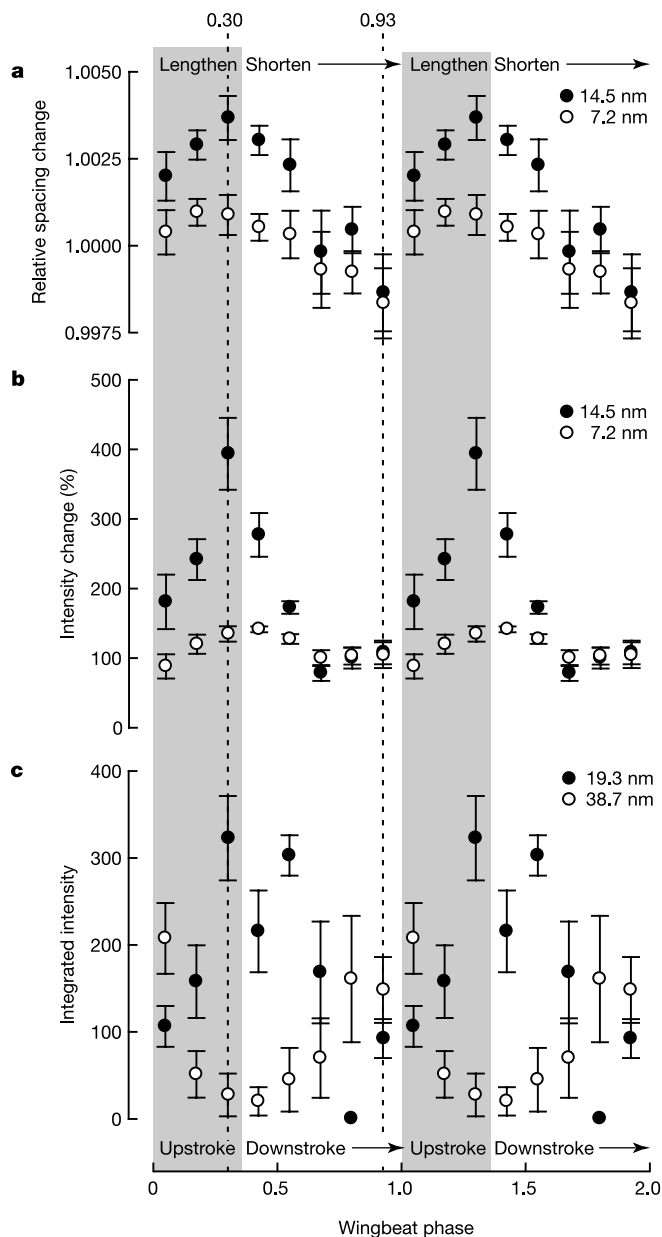


Figure 3 Changes in diffraction features as a function of phase of the wingbeat cycle. **a**, The 7.2-nm and 14.5-nm reflection spacings relative to rest. Thick-filament strain is approximately in phase with the wingbeat. **b**, The 7.2-nm and 14.5-nm reflection intensities relative to rest. A fourfold variation in the 14.5-nm reflection intensity is observed in phase with thick-filament strain. **c**, Integrated intensities of the first row line reflections on the 19.3-nm and 38.7-nm layer lines. Note the roughly reciprocal relation between the two intensities. Error bars show standard errors of the mean.

responsible for promoting stretch activation. In this view, it is the release in strain that causes all heads to detach abruptly, leading to shortening deactivation.

In these experiments we have coupled synchrotron X-ray diffraction with a tethered flight simulator to obtain an integrated picture of muscle structure and function within a living animal. The results of this time-resolved analysis shed light on two important features of the asynchronous flight muscle of insects. First, the strains measured within the stiff thick filaments might indicate a method by which lengthening flight muscles may store elastic energy for use in the next wingbeat. Second, changes in the number and orientation of crossbridge attachments throughout the wingbeat are likely to be instrumental in the process of stretch-activation. The crossbridge dynamics observed here provide constraints for future attempts to link the roughly 7-nm single myosin powerstrokes to the 50–60-nm movements of half sarcomeres within each 5-ms wingbeat cycle. Modifying the methods described here to enhance temporal resolution might help to address this question. *Drosophila* is ideally suited for these experiments, given its high degree of structural order and its suitability for future structure–function studies with genetic engineering methods²⁹. □

Methods

X-ray instrumentation

X-ray experiments used the small angle instrument on the BioCAT undulator-based beamline 18-ID (ref. 30) at the Advanced Photon Source, Argonne National Laboratory, Argonne, Illinois. The overall experimental arrangement is shown in Fig. 1. X-ray optics focus the beam horizontally at the fly and vertically at the detector. This optical arrangement allows the selection of these muscles to the exclusion of other nearby muscle systems. The X-ray beam energy was 12 keV (wavelength 0.103 nm), with a specimen-to-detector distance of 1.9 m. Diffraction patterns were recorded with a MAR 165 CCD detector (MARUSA). A rapid shutter set duration of exposure and beam intensity was adjusted appropriately in the range 10^{11} – 10^{13} photons s^{-1} with aluminium attenuators to obtain adequate counting statistics in the X-ray pattern with minimal radiation damage to the specimen.

Preparation of specimens

Flies (*Drosophila metleri* or *Drosophila melanogaster*) were grown under uncrowded conditions to increase the thickness of the muscle fibres intercepted by the X-ray beam. Before being mounted, flies (3–5-day-old females) were anaesthetized by being cooled to 4 °C with a thermoelectrically cooled stage. Flies were tethered by gluing a fine tungsten wire to the upper region of the thorax, permitting free movement of the head and wings during flight. Flies so tethered will spontaneously flap their wings for about 20–40 min. After recovery from anaesthesia (1 h), a fly was mounted with the long axis of its thorax perpendicular to the X-ray beam (head upwards) such that the 0.2-mm-wide collimated X-ray beam intersected the two parallel sets of DLM fibres located on both sides of the median plane of the thorax (Fig. 1). It was important to position the beam relatively low in the thorax so as to miss the fused thoracic–abdominal ganglion that contains the neuronal circuits driving the flight muscles, to reduce radiation damage to the nervous system and to reduce X-ray background from other structures.

Timing and synchronization

To maintain a steady wingbeat we used a ‘tethered flight simulator’ consisting of an optical wingbeat analyser that tracked the movements of the animal’s wings, and a panoramic electrical display that presented the animal with dynamic visual stimuli². Figure 1 shows a schematic diagram of the flight arena as installed in the X-ray diffraction apparatus. Using this apparatus, animals will fly for 30–120 min before they run out of energy stores. When placed in the arena, an infrared diode mounted at the top of the arena casts shadows of the animal’s wings on the two optical sensors of the wingbeat analyser, which track the back and forth motion of the wings within the wingbeat plane. From the raw analogue signals of these optical sensors, dedicated online circuitry determines the amplitude of both wings in each wingbeat as well as the instantaneous frequency. The visual display surrounding the animal consists of a cylindrical array of 16 light-emitting diode panels, each consisting of an 8 × 8 array of individual elements. Programmed images (bitmaps) are scanned onto the display at 1 kHz. In closed-loop mode, the behaviour of the animal (measured by the wingbeat analyser) is used to control the horizontal motion of the visual display that causes the fly to adjust its wingbeat frequency accordingly. The wingbeat analyser also provides a trigger pulse corresponding to a precise point in the wingbeat cycle about 1 ms before the start of the upstroke. A program running on a laptop computer was used to monitor the trigger pulse, to calculate the average wingbeat frequency from the running average of ten wingbeat periods and to trigger the shutter (opening time 340 μs), after a delay set to a preset fraction (‘phase’) of the wingbeat period, once for every ten wingbeats. Diffraction patterns consisted of the sum of 150 such exposures (52.5 ms total exposure). There were eight phases per wingbeat, so each phase was separated by about 0.6 ms.

Data analysis

Intensities of meridional reflections were estimated by integrating the area under the peaks in one-dimensional projections with the multiple one-dimensional fitting routines in the program FIT2D (<http://www.esrf.fr/computing/scientific/FIT2D>) assuming a polynomial background and gaussian peaks. For estimation of the 38.7-nm and 19.3-nm first row line reflection intensities, a radially symmetric background was subtracted from each pattern by using the routines in the XFIX program in the CCP13 suite (<http://www.ccp13.ac.uk>) before analysis.

Received 20 August; accepted 29 November 2004; doi:10.1038/nature03230.

- Josephson, R., Malamud, J. & Stokes, D. Asynchronous muscle: a primer. *J. Exp. Biol.* **203**, 2713–2722 (2000).
- Lehmann, F. O. & Dickinson, M. H. The changes in power requirements and muscle efficiency during elevated force production in the fruit fly *Drosophila melanogaster*. *J. Exp. Biol.* **200**, 1133–1143 (1997).
- Reedy, M. K., Holmes, K. C. & Tregear, R. T. Induced changes in orientation of the cross-bridges of glycerinated insect flight muscle. *Nature* **207**, 1276–1280 (1965).
- Miller, A. & Tregear, R. T. Evidence concerning crossbridge attachment during muscle contraction. *Nature* **226**, 1060–1061 (1970).
- Tregear, R. T. et al. X-ray diffraction indicates that active cross-bridges bind to actin target zones in insect flight muscle. *Biophys. J.* **74**, 1439–1451 (1998).
- al-Khayat, H. A., Yagi, N. & Squire, J. M. Structural changes in actin-tropomyosin during muscle regulation: computer modelling of low-angle X-ray diffraction data. *J. Mol. Biol.* **252**, 611–632 (1995).
- Reedy, M. K. & Reedy, M. C. Rigor crossbridge structure in tilted single filament layers and flared-X formations from insect flight muscle. *J. Mol. Biol.* **185**, 145–176 (1985).
- Taylor, K. A. et al. Tomographic 3D reconstruction of quick-frozen, Ca^{2+} -activated contracting insect flight muscle. *Cell* **99**, 421–431 (1999).
- Reedy, M. C. Visualizing myosin’s power stroke in muscle contraction. *J. Cell Sci.* **113**, 3551–3562 (2000).
- Irving, T. C. & Maughan, D. W. *In vivo* x-ray diffraction of indirect flight muscle from *Drosophila melanogaster*. *Biophys. J.* **78**, 2511–2515 (2000).
- Huxley, H. E. et al. Changes in the X-ray reflections from contracting muscle during rapid mechanical transients and their structural implications. *J. Mol. Biol.* **169**, 469–506 (1983).
- Irving, M., Lombardi, V., Piazzesi, G. & Ferenczi, M. A. Myosin head movements are synchronous with the elementary force-generating process in muscle. *Nature* **357**, 156–158 (1992).
- Irving, M. et al. Conformation of the myosin motor during force generation in skeletal muscle. *Nature Struct. Biol.* **7**, 482–485 (2000).
- Huxley, H. E., Stewart, A. & Irving, T. Spacing changes in the actin and myosin filaments during activation, and their implications. *Adv. Exp. Med. Biol.* **453**, 281–288 (1998).
- Huxley, H. E., Reconditi, M., Stewart, A. & Irving, T. What the higher order meridional reflections tell us. *Biophys. J.* **84**, 139a (2003).
- Chan, W. P. & Dickinson, M. H. *In vivo* length oscillations of indirect flight muscles in the fruit fly *Drosophila virilis*. *J. Exp. Biol.* **199**, 2767–2774 (1996).
- Wakabayashi, K. et al. X-ray diffraction evidence for the extensibility of actin and myosin filaments during muscle contraction. *Biophys. J.* **67**, 2422–2435 (1994).
- Weis-Fogh, T. in *XV Int. Congr. Entomol. (Royal Entomological Society, London, 8 to 16 July 1964)* (ed. Freeman, P.) 186–188 (XII International Congress of Entomology, London, 1965).
- Alexander, R. M. & Bennet-Clark, H. C. Storage of elastic strain energy in muscle and other tissues. *Nature* **265**, 380–390 (1977).
- Dickinson, M. H. & Lighton, J. R. Muscle efficiency and elastic storage in the flight motor of *Drosophila*. *Science* **268**, 87–90 (1995).
- Menetret, J. F., Schroder, R. R. & Hofmann, W. Cryo-electron microscopic studies of relaxed striated muscle thick filaments. *J. Muscle Res. Cell Motil.* **11**, 1–11 (1990).
- Dobbie, I. et al. Elastic bending and active tilting of myosin heads during muscle contraction. *Nature* **396**, 383–387 (1998).
- Squire, J. M. *The Structural Basis of Muscular Contraction* (Plenum, New York, 1981).
- Linari, M., Reedy, M. K., Reedy, M. C., Lombardi, V. & Piazzesi, G. Ca-activation and stretch-activation in insect flight muscle. *Biophys. J.* **87**, 1101–1111 (2004).
- Agianian, B. et al. A troponin switch that regulates muscle contraction by stretch instead of calcium. *EMBO J.* **23**, 772–779 (2004).
- Tregear, R. T. et al. Cross-bridge number, position, and angle in target zones of cryofixed isometrically active insect flight muscle. *Biophys. J.* **86**, 3009–3019 (2004).
- Juanhuix, J. et al. Axial disposition of myosin heads in isometrically contracting muscles. *Biophys. J.* **80**, 1429–1441 (2001).
- Littlefield, K. P. et al. The converter domain modulates kinetic properties of *Drosophila* myosin. *Am. J. Physiol. Cell Physiol.* **284**, C1031–C1038 (2003).
- Sparrow, J., Drummond, D., Peckham, M., Hennessey, E. & White, D. Protein engineering and the study of muscle contraction in *Drosophila* flight muscles. *J. Cell Sci. Suppl.* **14**, 73–78 (1991).
- Irving, T. C., Fischetti, R. E., Rosenbaum, G. & Bunker, G. B. Fiber diffraction using the BioCAT Undulator Beamline at the Advanced Photon Source. *Nucl. Instrum. Methods A* **448**, 250–254 (2000).

Supplementary Information accompanies the paper on www.nature.com/nature.

Acknowledgements We thank J. Costello for help with data analysis, J. Fockler for computer programming, and D. Swank, R. Tregear, M. K. Reedy and M. C. Reedy for helpful discussions. The research was supported by NIH. The APS is supported by the US Department of Energy. BioCAT is a NIH-supported Research Center.

Competing interests statement The authors declare that they have no competing financial interests.

Correspondence and requests for materials should be addressed to T.I. (irving@iit.edu).